

## Discovery and Mechanism of Action studies of 4,6-diphenylpyrimidine-2-carbohydrazides as utrophin modulators for the treatment of Duchenne muscular dystrophy

Aini Vuorinen<sup>1\*</sup>, Isabel V.L. Wilkinson<sup>1\*</sup>, Maria Chatzopoulou<sup>1</sup>, Ben Edwards<sup>2</sup>, Sarah E. Squire<sup>2</sup>, Rebecca J. Fairclough<sup>2§</sup>, Noelia Araujo Bazan<sup>1</sup>, Josh A. Milner<sup>1</sup>, Daniel Conole<sup>1</sup>, James R. Donald<sup>1</sup>, Nandini Shah<sup>2</sup>, Nicky J. Willis<sup>1</sup>, Fernando Martinez Vazquez<sup>1</sup>, Francis X. Wilson<sup>3</sup>, Graham M. Wynne<sup>1</sup>, Stephen G. Davies<sup>1</sup>, Kay E. Davies<sup>2†</sup>, Angela J. Russell<sup>1,4†</sup>

\*Joint first authors, †corresponding authors, [angela.russell@chem.ox.ac.uk](mailto:angela.russell@chem.ox.ac.uk);  
[kay.davies@dpag.ox.ac.uk](mailto:kay.davies@dpag.ox.ac.uk).

<sup>1</sup>Department of Chemistry, University of Oxford, Chemistry Research Laboratory, Mansfield Road, Oxford, OX1 3TA, UK; <sup>2</sup>Department of Physiology, Anatomy and Genetics, University of Oxford, Sir Henry Wellcome Building of Gene Function, South Parks Road, Oxford, OX1 3PT, UK; <sup>3</sup>Summit Therapeutics plc., 136a Eastern Avenue, Milton Park, Abingdon, Oxfordshire, OX14 4SB, UK; <sup>4</sup>Department of Pharmacology, University of Oxford, Mansfield Road, Oxford, OX1 3PQ, UK.

<sup>§</sup>Current address: Emerging Innovations Unit, AstraZeneca.

### Abstract

Duchenne muscular dystrophy is a fatal disease with no cure, caused by lack of the cytoskeletal protein dystrophin. Upregulation of utrophin, a dystrophin paralogue, offers a potential therapy independent of mutation type. The failure of first-in-class utrophin modulator ezutromid/SMT C1100 in Phase II clinical trials necessitates development of compounds with better efficacy, physicochemical and ADME properties and/or complementary mechanisms. We have discovered and performed a preliminary optimisation of a novel class of utrophin modulators using an improved phenotypic screen, where reporter expression is derived from the full genomic context of the utrophin promoter. We further demonstrate through target deconvolution studies, including expression analysis and chemical proteomics, that this compound series operates via a novel mechanism of action, distinct from that of ezutromid.

**Keywords** Duchenne muscular dystrophy, utrophin, phenotypic drug discovery, mechanism of action, target deconvolution, chemical proteomics, photoaffinity labelling

### Introduction

Duchenne muscular dystrophy (DMD) is an X-linked progressive muscle-wasting disease caused by a lack of the cytoskeletal protein dystrophin. There is currently no disease modifying treatment for all patients, although various promising approaches (e.g. exon skipping, readthrough of stop codons and gene therapy) are being developed and are starting to be approved for clinical use in certain patient cohorts [1]. Oral small molecules have been developed to compensate for the missing dystrophin by replacing it with its autosomal paralogue utrophin [2]. This therapy would be applicable to all patients regardless of their dystrophin mutation and would be systemically bioavailable.

The first-in-class utrophin modulator, ezutromid (formerly SMT C1100), was developed using a high throughput cell-based phenotypic screen [3]. The screening cell line consisted of

immortalized murine DMD disease model (*mdx*) myoblasts transfected with 8.4 kb of the human utrophin A promoter upstream of firefly luciferase (H2K-*mdx* utrA-luc, Figure 1a) [4]. Evaluation of ezutromid in a Phase II clinical trial in DMD patients revealed encouraging signs of on-target activity, including reduced muscle fibre damage and increased levels of utrophin, at the trial midpoint [2]. However, ezutromid is susceptible to CYP-mediated metabolism [5] and rapid clearance in patients [6], and its therapeutic benefits were not sustained through to the end of the trial, leading to discontinuation of its clinical development. Therefore, utrophin modulators with improved efficacy, physicochemical and ADME properties and/or complementary mechanisms of action are now required. Here we describe a novel class of small molecule utrophin modulators, discovered in a new screening cell line, that operate via a previously undescribed mode of action, as proven by expression analysis and chemoproteomics.

## Results and Discussion

A cell-based reporter system which exploits the full utrophin promoter in its endogenous genomic context and encompassing all known utrophin isoforms and regulatory elements was developed by knock-in of firefly luciferase into one *UTRN* exon 7 of a dystrophin-null mouse (LU*mdx*; *mdx*, *utr*<sup>luc/+</sup>, Figure 1b, procedure described in the Experimental Methods). 7000 drug-like small molecules from our in house compound collection were screened in immortalised myoblasts from the LU*mdx* mouse. After counterscreening for firefly luciferase assay interference [7,8] to ensure genuine activation of the utrophin promoter, this screen gave rise to several novel hit series' of utrophin modulators.

Interestingly, one of these compounds, an unusual heteroaryl acyl hydrazide denoted OX01914 (**1**, Figure 1f), demonstrated activity in the new LU*mdx* reporter cell line, but not the original H2K-*mdx* utrA-luc screening cell line [4] (Figure 1c), with the activity confirmed to be independent of luciferase interference (Supplementary Figure 1a-b). This finding suggested that OX01914 may operate via a mechanism of action which is distinct from that of ezutromid, which we recently reported to be mediated by the antagonism of the aryl hydrocarbon receptor [9].

The ability of OX01914 to upregulate utrophin mRNA in LU*mdx* and H2K *mdx* myoblasts was confirmed by qPCR, with a 2-fold increase observed at the highest dose in LU*mdx* (Figures 1d and 2). Next, upregulation of utrophin expression by OX01914 was investigated in human DMD muscle cells at the protein level. Excitingly, OX01914 treatment led to a statistically significant 3-fold increase in utrophin protein expression (Figure 1e), far in excess of the 1.5 fold increase along the membrane required to see a beneficial effect [2]. On the basis of these encouraging results in *mdx* and DMD muscle cells, the physicochemical/ADME properties of OX01914 were assessed to guide compound optimisation. OX01914 demonstrated good aqueous solubility and permeability, however, was rapidly metabolised by mouse hepatocytes ( $T_{1/2}$  3 min) – a profile that was also sustained in human hepatocytes ( $T_{1/2}$  28 min, Figure 1g).

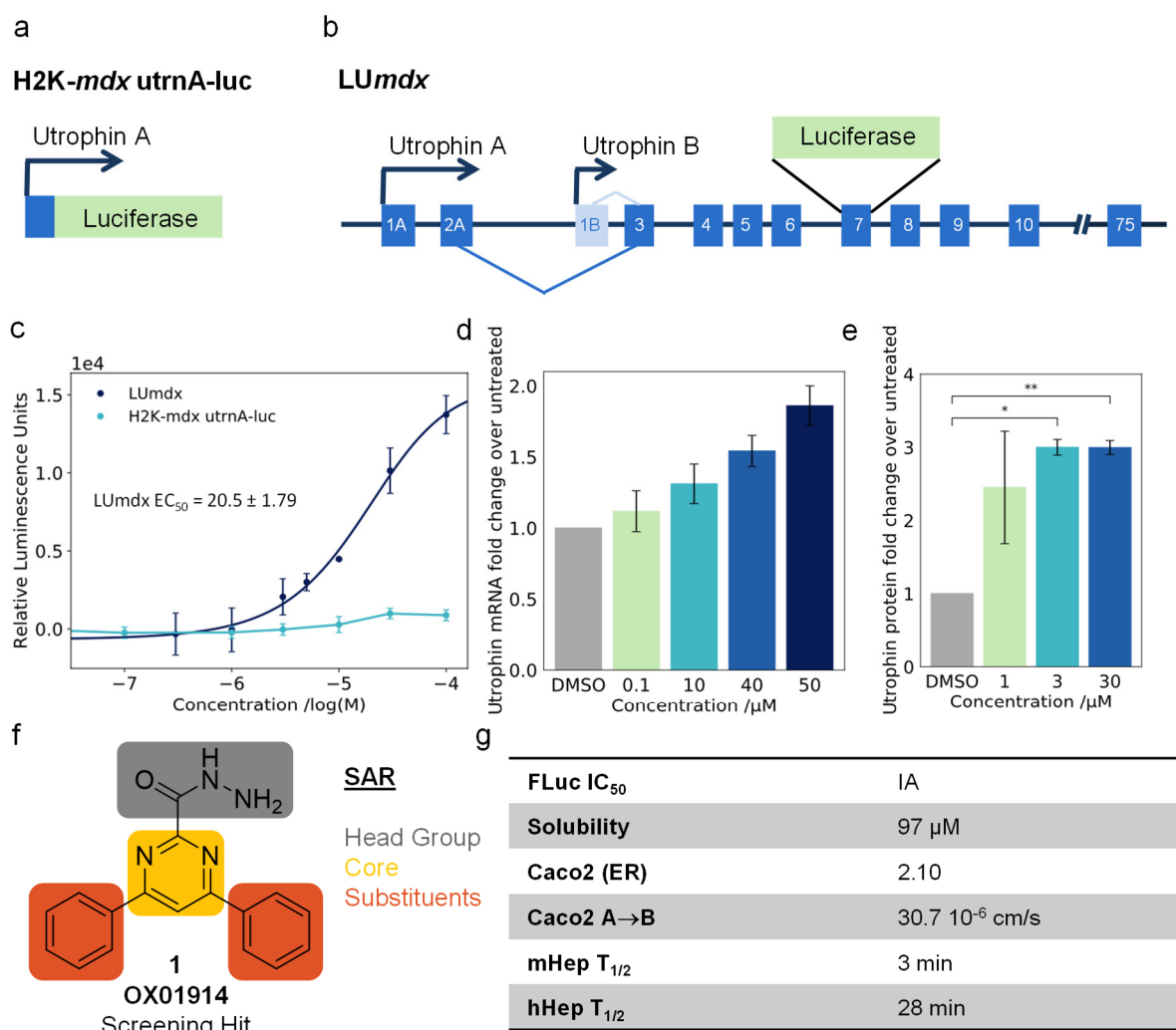


**Figure 1** Schematic of firefly luciferase reporter gene assay phenotypic screens for utrophin gene upregulation: a) H2K-*mdx* utrA-luc cell line, b) LU*mdx* cell line; c) OX01914 (**1**) activates luciferase in the LU*mdx* cell line but not in H2K-*mdx* utrA-luc line, N = 3, representative graph shown; d) OX01914 increases utrophin mRNA levels in LU*mdx* myoblasts, n = 2, see also Figure 2; e) OX01914 increases utrophin protein levels by approximately 3-fold, N = 2; f) structure of OX01914 and areas of interest for structure-activity relationships; g) luciferase inhibition, physicochemical and ADME properties of OX01914. Solubility: aqueous thermodynamic solubility, Caco2 permeability efflux ratio (ER) and apical to basolateral (A→B) transport, mHep T<sub>1/2</sub>: half-life in mouse hepatocytes and hHep T<sub>1/2</sub>: half-life in human hepatocytes.

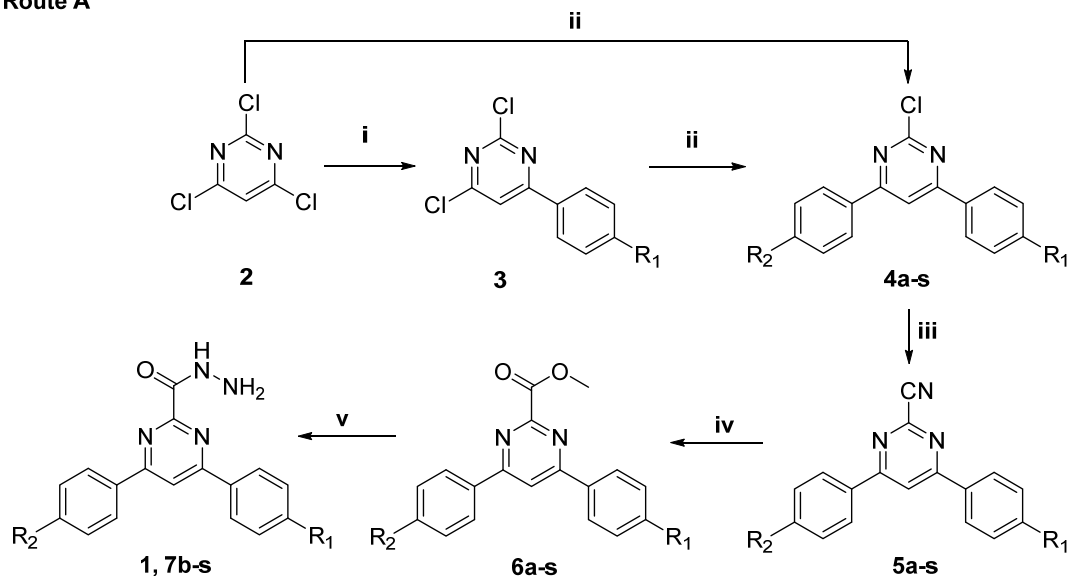
## Chemistry

As part of the hit confirmation process, and to establish a synthetic route to further analogues, resynthesis of OX01914 was undertaken (Route A, Scheme 1, synthesis of analogues using Route A detailed in Scheme S1). In an initial Suzuki reaction using an excess of 2,4,6-trichloropyrimidine **2**, selective monosubstitution to afford **3** was achieved in good yield (82%). The second Suzuki coupling to form disubstituted chlorides **4** was also high yielding (61-76%), apart from some analogues bearing a free OH group (36 and 42% for **4k** and **4r**, respectively).

Symmetrical analogues were synthesised with 2 equivalents of boronic acid. DABCO-mediated displacement of the 2-chloro substituent yielded nitriles **5** in mostly moderate to good yields (52-91%), barring once more analogues bearing a free OH group (50% and 46% for **5k** and **5r**, respectively). Methanolysis of nitriles **5** provided the methyl esters **6** and treatment with hydrazine resulted in the desired hyrazides **7** in moderate to good yields (44-96%).

**Scheme 1.** Routes employed towards synthesis of hit compound OX01914 and analogues

### Route A



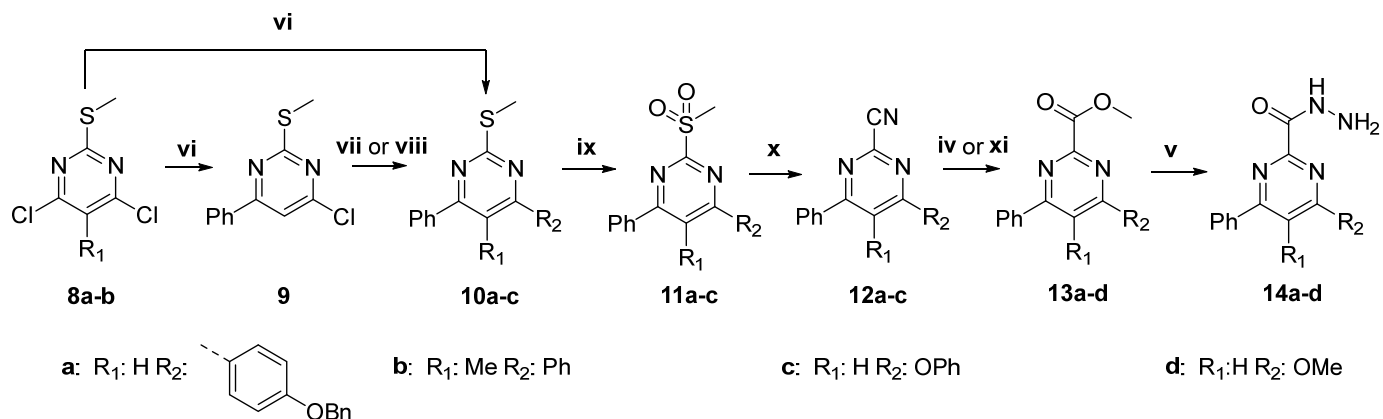
**a:** R<sub>1</sub>,R<sub>2</sub>: H  
**b:** R<sub>1</sub>,R<sub>2</sub>: 2-F  
**c:** R<sub>1</sub>,R<sub>2</sub>: 3-F  
**d:** R<sub>1</sub>,R<sub>2</sub>: 4-F  
**e:** R<sub>1</sub>,R<sub>2</sub>: 2-OMe

**f:** R<sub>1</sub>,R<sub>2</sub>: 3-OMe  
**g:** R<sub>1</sub>,R<sub>2</sub>: 4-OMe  
**h:** R<sub>1</sub>,R<sub>2</sub>: 2-CF<sub>3</sub>  
**i:** R<sub>1</sub>,R<sub>2</sub>: 3-CF<sub>3</sub>  
**j:** R<sub>1</sub>,R<sub>2</sub>: 4-CF<sub>3</sub>

**k:** R<sub>1</sub>: H R<sub>2</sub>: 4-OH  
**l:** R<sub>1</sub>: H R<sub>2</sub>: 4-OMe  
**m:** R<sub>1</sub>: H R<sub>2</sub>: 4-OEt  
**n:** R<sub>1</sub>: H R<sub>2</sub>: 4-O<sup>n</sup>Pr  
**o:** R<sub>1</sub>: H R<sub>2</sub>: 4-O<sup>n</sup>Bu

**p:** R<sub>1</sub>: H R<sub>2</sub>: 4-OPh  
**q:** R<sub>1</sub>: H R<sub>2</sub>: 4-<sup>n</sup>Pr  
**r:** R<sub>1</sub>: H R<sub>2</sub>: 4-CH<sub>2</sub>OH  
**s:** R<sub>1</sub>: H R<sub>2</sub>: 4-OCH<sub>2</sub>CH<sub>2</sub>OMe

### Route B



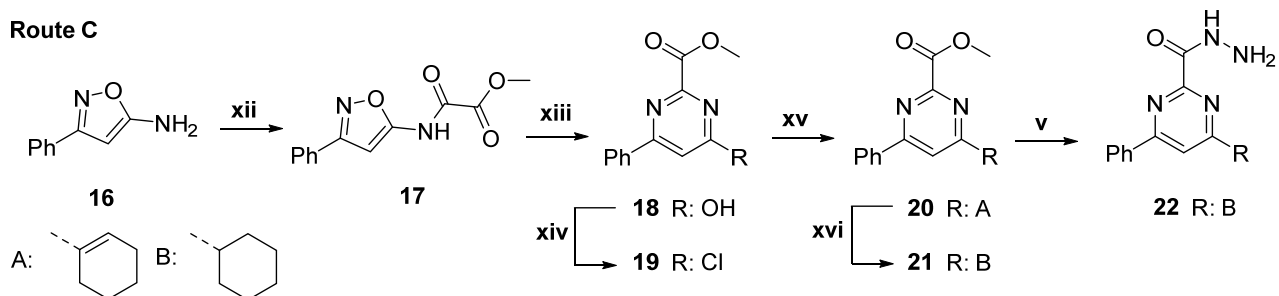
**a:** R<sub>1</sub>: H R<sub>2</sub>:

**b:** R<sub>1</sub>: Me R<sub>2</sub>: Ph

**c:** R<sub>1</sub>: H R<sub>2</sub>: OPh

**d:** R<sub>1</sub>: H R<sub>2</sub>: OMe

### Route C



**A:** **B:**

**Reagents and conditions:** i) R<sub>1</sub>-arylboronic acid (1 eq), Pd(OAc)<sub>2</sub>, PPh<sub>3</sub>, Na<sub>2</sub>CO<sub>3</sub>, DME/H<sub>2</sub>O, 85 °C, 24 h; ii) R<sub>2</sub>-arylboronic acid, Pd(OAc)<sub>2</sub>, PPh<sub>3</sub>, Na<sub>2</sub>CO<sub>3</sub>, DME/H<sub>2</sub>O, 85 °C, 24 h; iii) KCN, DABCO, DMSO/H<sub>2</sub>O, 80 °C, 1-3 h; iv) AcCl, MeOH, 65 °C, 2-3 h; v) NH<sub>2</sub>NH<sub>2</sub>·H<sub>2</sub>O, PhMe/EtOH, rt, 24 h; vi) Phenylboronic acid (1 or 2.5 eq), Pd(PPh<sub>3</sub>)<sub>4</sub>, 2 M K<sub>2</sub>CO<sub>3</sub>, PhMe, 95 °C, 24 h; vii) arylboronic acid, Pd(OAc)<sub>2</sub>, PPh<sub>3</sub>, Na<sub>2</sub>CO<sub>3</sub>, DME/H<sub>2</sub>O, 85 °C, 24 h; viii) PhOH,

CsCO<sub>3</sub>, MeCN, rt, 60 h; ix) Oxone®, CH<sub>3</sub>CN/PhMe/H<sub>2</sub>O, 60 °C, 3 d; x) KCN, DMSO, rt, 24 h; xi) MeONa, MeOH/PhCH<sub>3</sub>, 10 °C to rt, 3 h; xii) ClCOCOOMe, pyridine, 0 °C, 1 h; xiii) PtO<sub>2</sub>, H<sub>2</sub>, EtOH, rt, 3 h; xiv) POCl<sub>3</sub>, PhNMe<sub>2</sub>, 100 °C, 3 h; xv) cyclohex-1-en-1-ylboronic acid, Pd(PPh<sub>3</sub>)<sub>4</sub>, 2 M K<sub>2</sub>CO<sub>3</sub>, PhMe, 80 °C, 3 h; xvi) H<sub>2</sub>, Pd/C (10% wt), EtOAc, rt, 3 h.

OX01914 analogues bearing a free phenol could act as important key intermediates for further functionalisation. However, synthetic Route A provided phenol analogues such as **7k** (Scheme 1) with low overall yields (6%, full synthesis details described in the Supporting Information). Use of the *O*-benzyl protecting group significantly improved the Suzuki coupling yield, however the subsequent displacement with cyanide led to a mixture of unidentified products (data not shown). An alternative strategy was therefore pursued, replacing the 2-chloro substituent with a 2-thiomethyl group **8** to be further oxidised (**11**) and displaced with cyanide **12** (Route B, Scheme 1). Employing a *N*-Boc-protecting group on the hydrazide allowed functionalisation at the phenolic OH without competing nucleophilic reaction of the hydrazide (Scheme S2). Though longer, this synthetic sequence allowed the synthesis of key intermediate **N-Boc-7k** on a 3 gram scale in 37% yield over 8 steps. This route was also used to synthesise OPh analogue **14c** for the investigation of substituent effect on the pyrimidine ring. OMe analogue **14d** was the adventitious product of nitrile methanolysis during the synthesis of **14c**, arising from displacement of the phenoxy group with methanol. Adopting milder conditions with MeONa allowed access to the desired OPh analogue **14c**.

In addition, a shorter synthesis (Route C, Scheme 1) was investigated to access cyclohexyl analogue **22** in 6 steps. First, 3-phenylisoxazol-5-amine **16** was treated with methyl oxalyl chloride and the product cyclised to 4-hydroxypyrimidine **18**. POCl<sub>3</sub> displacement of the hydroxy group with chloride allowed for a palladium coupling with cyclohexene to give **20**. Olefin **20** was then hydrogenated and treated with hydrazine hydrate to provide the cyclohexyl analogue **22**. Advantageously, this route could accelerate SAR development on one aryl ring at a time.

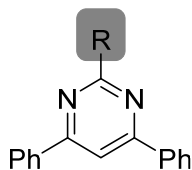
### Structure-activity relationships around OX01914

Seeking to establish the minimum structural moieties required for activity (Figure 1f), we investigated (i) a small range of head group replacements (Table 1), (ii) alterations of the pyrimidine core (Table 2), (iii) the role of the substituents on the 4,6-positions of the pyrimidine ring (Table 3) and (iv) the influence of regiochemistry on the phenyl rings (Table 4).

Leveraging chloride intermediate **4a** from Route A to **OX01914** allowed for rapid synthesis of head group variants including hydrazine analogue **23** and methylene linked hydrazide analogue **25** (Table 1, Scheme S3). Meanwhile, the methyl ester intermediate **6a** allowed facile synthesis of amide **26**, carboxylic acid **27** and a hydroxamic acid analogue **28** (Table 1, Scheme S3). Finally, imide analogue **30** was synthesised from **6a** in three steps: reduction to an alcohol (**29**, Scheme S3), Dess-Martin periodinane-mediated oxidation to an aldehyde then reaction with hydrazine.

Intriguingly, these alterations on the head group were not tolerated, with hydrazine analogue **23**, methylene linked analogue **25**, methyl ester intermediate **6a** and imide analogue **30** all inactive in the LUmdx reporter gene assay when tested at concentrations up to 100 μM. Even more subtle alterations including to amide, carboxylic acid and hydroxamic acid moieties led to inactive analogues (Table 1).

**Table 1.** Preliminary structure – activity relationships on the head group, N (biological replicates)  $\geq 2$ , n (technical replicates) =3, IA = inactive.

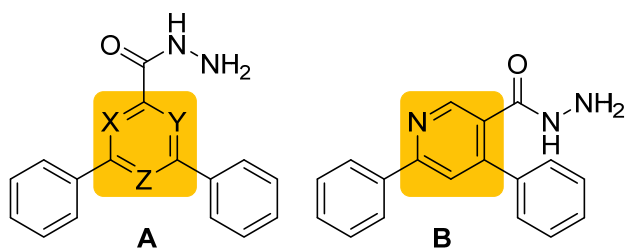


#	R	EC <sub>50</sub> ± SEM ( $\mu$ M)
1	CONHNH <sub>2</sub>	20.5 ± 1.79
23	NHNH <sub>2</sub>	IA
25	CH <sub>2</sub> CONHNH <sub>2</sub>	IA
6a	COOMe	IA
26	CONH <sub>2</sub>	IA
27	COOH	IA
28	CONHOH	IA
30	CH=NNH <sub>2</sub>	IA

To investigate the SAR of the core scaffold, pyridine analogues **33** and **40**, as well as regioisomeric pyrimidine **34** were synthesised from the respective 4,6-dichloro-2-carboxylate esters in two steps: Suzuki coupling followed by treatment with hydrazine hydrate (Scheme S4). Triazine analogue **38** was synthesised from 2,4,6-trichlorotriazine in a similar sequence to the **OX01914** analogues in Scheme S1 (Scheme S4).

However, alterations to the structure of **OX01914** led to a loss of activity, except in the case of triazine analogue **38**, which was found to give comparable or somewhat improved activity compared to the original hit **1** (Table 2). In this study we continued to focus on optimisation of the pyrimidine core. The large effect on activity of relatively subtle structural alterations was interesting to note, for example, the introduction of a methyl substituent at the 5 position of the pyrimidine ring which led to inactive analogue **14b**. As such, 5-methylated pyrimidine acyl hydrazides can be usefully employed as negative controls in assay development and target deconvolution studies.

**Table 2.** Preliminary structure – activity relationships on the core, N  $\geq 1$  (biological replicate), n=3 (technical replicates), IA = inactive.

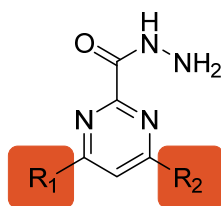


#	X	Y	Z	Scaffold	EC <sub>50</sub> ± SEM (μM)
1	N	N	CH	A	20.5 ± 1.79
33	N	CH	CH	A	IA
34	N	CH	N	A	IA
38	N	N	N	A	8.98*
40	-	-	-	B	IA
14b	N	N	C-Me	A	IA

\* R<sup>2</sup> = 0.91 (goodness of fit where only technical replicates were performed)

Next, recognising the desirability of steering away from flat polyaromatic molecules [10] we investigated introducing more 3D structure, by replacing one or both aromatic substituents with methyl substituents, oxygen-linkers and a cyclohexyl substituent (Table 3, synthesis described in Scheme 1). All of these modifications led to inactive analogues.

**Table 3.** Preliminary structure – activity relationships on the substituents, N ≥ 2 (biological replicates), n=3 (technical replicates), IA = inactive.



#	R <sup>1</sup>	R <sup>2</sup>	EC <sub>50</sub> ± SEM (μM)
1	Ph	Ph	20.5 ± 1.79
41*	H	H	IA
42*	Me	Me	IA
14c	OPh	Ph	IA
14d	OMe	Ph	IA
22	cyclohexyl	Ph	IA

\*Obtained commercially

**Table 4.** Investigation of phenyl ring regiochemistry to determine the optimal position for substitution on hit compound OX01914. N = 1 (biological replicate), n=3 (technical replicates). IA = inactive, R<sup>2</sup> indicates goodness of fit where only technical replicates were performed.



#	R	EC <sub>50</sub> ± SEM (µM)	R <sup>2</sup>
<b>1</b>	Ph	20.5 ± 1.79	
<b>7b</b>	2-F	11.0	0.94
<b>7c</b>	3-F	>10	0.88
<b>7d</b>	4-F	12.8	0.96
<b>7e</b>	2-OMe	IA	
<b>7f</b>	3-OMe	9.22	0.56
<b>7g</b>	4-OMe	7.14	0.95
<b>7h</b>	2-CF <sub>3</sub>	IA	
<b>7i</b>	3-CF <sub>3</sub>	IA	
<b>7j</b>	4-CF <sub>3</sub>	>10	0.95

Finally, several analogues bearing substituted phenyl rings (Table 4, **7b-7j**) were synthesised to delineate the effect of peripheral regiochemistry on activity. Symmetrical analogues were chosen for this investigation due to their facile synthesis (Route A). Small substituents like fluorine maintained activity regardless of regiochemistry, while *meta*- and *para*-methoxy groups were also tolerated. Interestingly, *ortho*- and *meta*-CF<sub>3</sub> substitution both led to loss of activity, while the *para* position tolerated the widest range of substituents.

### Mechanism of action studies

To confirm that OX01914 (**1**) upregulates utrophin expression via a mechanism distinct from that of the AhR antagonist ezutromid, qPCR of utrophin and AhR was undertaken in H2K *mdx* myoblasts (Figure 2). Both ezutromid (3 µM) and OX01914 (30 µM) significantly increased utrophin mRNA levels compared to DMSO control (1.7 and 1.6 fold respectively). However, while ezutromid increased AhR mRNA levels approximately 2 fold, consistent with AhR antagonism and in accordance with previous reports [11], OX01914 treatment did not result in any significant difference in AhR expression. This result supports the hypothesis that ezutromid and OX01914 upregulate utrophin through different mechanisms.

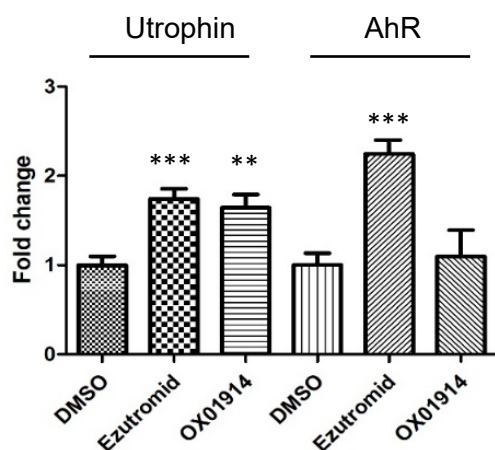


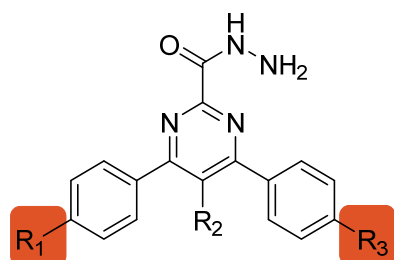
**Figure 2.** Both ezutromid (3  $\mu\text{M}$ ) and OX01914 (30  $\mu\text{M}$ ) upregulate utrophin mRNA expression in H2K *mdx* myoblasts, but only ezutromid upregulates AhR expression (N biological replicates = 2, n = 3 technical replicates). \*\* and \*\*\* indicate p-values of <0.005 and <0.0005 respectively.

Target identification can greatly assist lead optimisation by enabling structure activity relationship (SAR) studies to be conducted more efficiently and rationally [12,13]. Furthermore, identification of on- and off-targets can allow optimisation to reduce side effects, increase efficacy and find new applications for the compounds. Here, a chemical proteomics strategy using cell-permeable photoaffinity-labelled clickable probes [14] was employed to identify proteins targeted by the OX01914 chemotype.

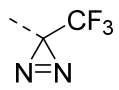
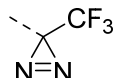
Use of a photoaffinity label can allow identification of even weakly bound proteins, by enabling UV-mediated covalent binding of the probe to its protein target [15]. A trifluoromethylphenyl diazirine (TPD) was selected as the photoaffinity label, with its placement 'nested' within the structure of OX01914 to minimise structural perturbation [16]. Substitution of the diazirine in the *para* position was informed by the SAR for the series (Table 5). Synthesis of trifluoromethylphenyl diazirines from the corresponding ketones is well-established [16] and was performed over 4 steps for the synthesis of diazirine-labelled probes **63-65** (Scheme S6). *N*-Boc-protection was employed for the installation of the acyl hydrazine after diazirine synthesis as without it hydrazine was found to reduce the diazirine ring back to the diazididine.

Gratifyingly, photoaffinity probe **63** was found to have good activity (Table 5,  $\text{EC}_{50} = 7.22 \pm 0.72 \mu\text{M}$ ) in the utrophin promoter reporter gene assay.

**Table 5.** Structure – activity relationships for the synthesis of photoaffinity click probes, N  $\geq 2$  biological replicates, n=3 technical replicates, IA = inactive.



#	R <sub>1</sub>	R <sub>2</sub>	R <sub>3</sub>	EC <sub>50</sub> ± SEM ( $\mu\text{M}$ )
<b>1</b>	H	H	H	20.5 ± 1.79
<b>7k</b>	OH	H	H	1.57 ± 0.24
<b>7l</b>	OMe	H	H	2.28 ± 0.09
<b>7m</b>	OEt	H	H	2.71 ± 0.30
<b>7n</b>	O <sup>n</sup> Pr	H	H	5.62 ± 0.09
<b>7o</b>	O <sup>n</sup> Bu	H	H	IA
<b>7p</b>	OPh	H	H	IA
<b>7q</b>	<sup>n</sup> Pr	H	H	4.54 ± 0.57
<b>7r</b>	CH <sub>2</sub> OH	H	H	1.90 ± 0.34
<b>7t</b>	CH <sub>2</sub> OMe	H	H	4.65 ± 0.50
<b>7s</b>	OCH <sub>2</sub> CH <sub>2</sub> OMe	H	H	8.95 ± 1.02
<b>7u</b>	OCH <sub>2</sub> CH <sub>2</sub> OBn	H	H	IA
<b>49</b>	OCH <sub>2</sub> CH <sub>2</sub> OCH <sub>2</sub> CH <sub>2</sub> NHAc	H	H	12.7 ± 1.57
<b>50</b>	OCH <sub>2</sub> CH <sub>2</sub> OCH <sub>2</sub> C≡CH	H	H	14.9 ± 1.17
<b>63</b>	H	H		7.22 ± 0.72

<b>64</b>	OCH <sub>2</sub> CH <sub>2</sub> OCH <sub>2</sub> C≡CH	H		20.0 ± 2.29
<b>65</b>	OCH <sub>2</sub> CH <sub>2</sub> OCH <sub>2</sub> C≡CH	Me		IA

A click handle was desired for attachment of a purification tag such as biotin, and an alkyne was chosen for use in the well-precedented biorthogonal copper-catalysed azide-alkyne cycloaddition (CuAAC) reaction [17]. A polyethylene glycol (PEG) chain linker was also desired to improve accessibility of the alkyne for efficient CuAAC [18]. Different functionalities were introduced to see how steric effects and hydrophilic/hydrophobic groups were tolerated (Table 5). Initially the length of an *n*-alkoxy chain was increased systematically from methoxy to *n*-butoxy (**7i-7o**) and it was compared to its *para*-hydroxy substituted counterpart **7k**. Compounds **7q-7t** were then prepared to see how the presence of oxygen and its position affects the activity. Additionally, compounds **7p**, and **7u** were prepared to explore steric effects.

In the alkoxy-substituted series (**7i-7o**) activity is maintained until the *n*-propoxy analogue **7n**, though somewhat diminished, but the bulkier *n*-butoxy and phenoxy (**7o** and **7p**, respectively) were both inactive. Interestingly, the ethylene glycol analogue **7s**, was active ( $EC_{50} \sim 9\mu\text{M}$ ), suggesting the incorporation of a polar atom within the chain is favourable for activity, when the length of the chain is increased.

Compounds **7k** and **7r** bearing a hydroxy group gave promising results with the lowest  $EC_{50}$  values (1.57  $\mu\text{M}$  and 1.90  $\mu\text{M}$ , respectively) and the methoxymethyl variant **7t** gave an  $EC_{50}$  of 4.65  $\mu\text{M}$ . These results show that the position of the oxygen atom along the chain can be changed with no loss in activity. Synthesis of PEG-chain variants **49** and the alkyne variant **50** proceeded smoothly from intermediate **N-Boc-7k** via an etherification reaction with the respective mesylated alcohols [19–21] and subsequent *N*-Boc-deprotection (Scheme S5). Importantly, **49** and **50** were both active in the low micromolar range ( $EC_{50}$ s of 12.7 and 14.9  $\mu\text{M}$ , respectively).

Ultimately, combination of the PEG alkyne and diazirine photoaffinity groups in dual-tagged probe **64** (Figure 3a) resulted in activity ( $EC_{50} = 20.0 \pm 2.29 \mu\text{M}$ , Table 5) comparable to that of OX01914. Noting the inactivity of 5-methylpyrimidine analogues of OX01914 such as **14b**, dual-tagged probe **65** (Figure 3a, Table 5) was also synthesised to serve as a negative control (synthesis of both probes reported in Scheme S6).

With both active and negative control probes in hand, their protein-interaction profiles were assessed with gel-based labelling experiments using live dystrophic mouse myoblasts. Both probes **64** and **65** (6.25 – 50  $\mu\text{M}$ ), were treated alongside DMSO vehicle for 2 h. After irradiation (365 nm) and cell lysis, the probe-labelled lysate was subjected to a CuAAC-mediated click reaction with TAMRA-azide, then SDS-PAGE. In-gel fluorescence showed dose-dependent labelling of proteins (Figure 3b), with no labelling apparent in the vehicle control.

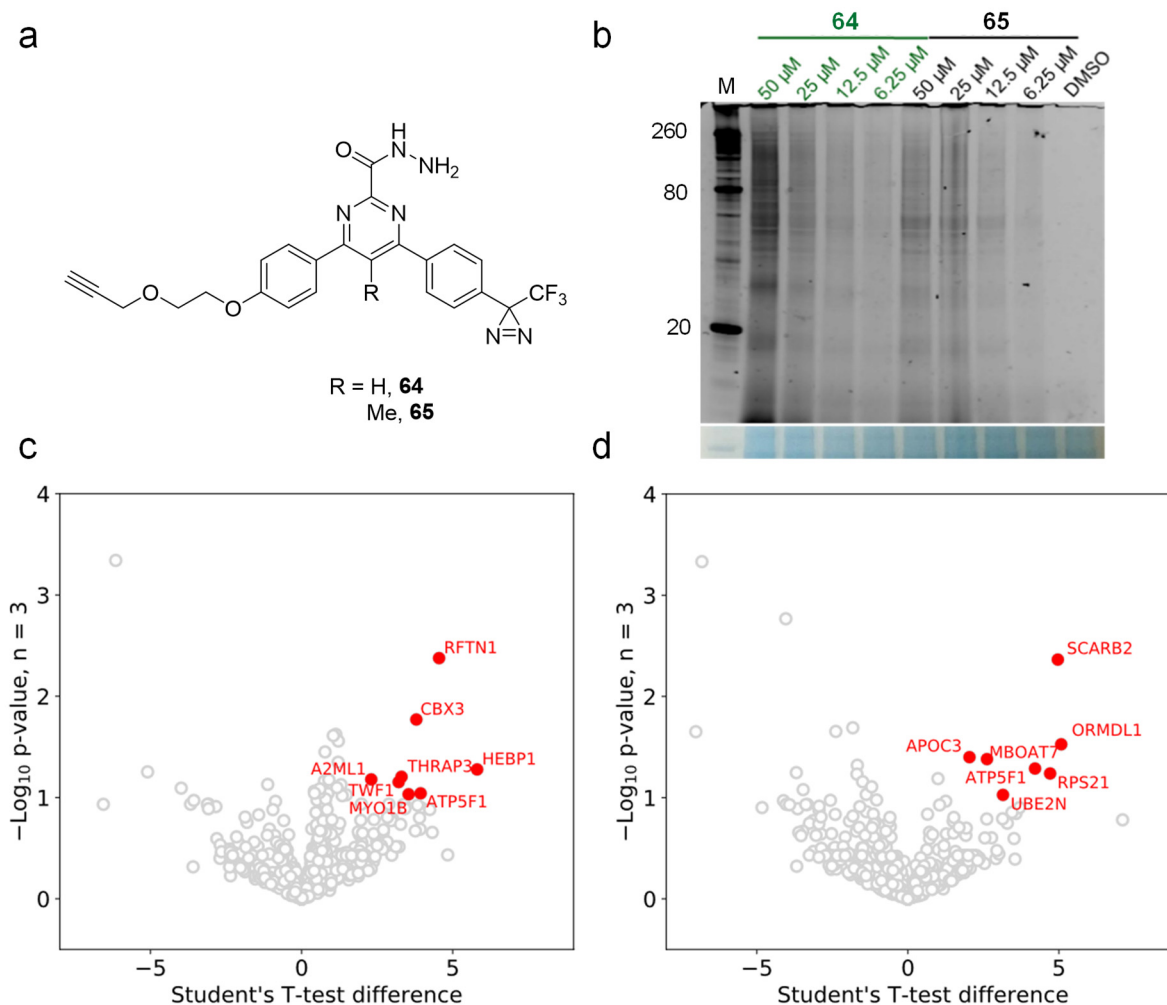


**Figure 3.** Target identification via chemical proteomics for the OX01914 chemotype. a) Structures of active **64** and inactive **65** photoaffinity-labelled clickable probes of OX01914; b) In-gel fluorescence of active and inactive probe-labelled H2K *mdx* proteome; c) Volcano plot of proteins enriched by active probe **64** in the presence and absence of competitor OX01914, top hits in red; d) Volcano plot of proteins enriched by active probe **64** compared to inactive probe **65**, top hits in red.

Protein target identification was next performed in live human DMD myoblasts using the two probes (30  $\mu\text{M}$ ). In addition, control samples were pre-treated with an excess concentration of the unmodified compound OX01914 (50  $\mu\text{M}$ ) to occupy the target binding sites and help distinguish non-specifically binding proteins. Probe-labelled proteins were clicked to azide-biotin, then enriched using streptavidin beads. Enriched proteins underwent on-bead tryptic digest and the peptides analysed by nano liquid chromatography-tandem mass spectrometry (nanoLC-MS/MS). Evaluation of proteins enriched by active probe **64** but displaced in the presence of the parent compound OX01914 delivered a shortlist of potential OX01914 targets (red proteins, Figure 3c). Meanwhile, proteins enriched by the active probe **64** but not the structurally similar inactive probe **65** are likely to mediate the therapeutic effects of the OX01914 chemotype (Figure 3d, full list of proteins identified available in Supplementary Information). As anticipated, unlike as was previously seen for ezutromid-based photoaffinity probes [9], the aryl hydrocarbon receptor was not detected by these acyl hydrazide probes, supporting the hypothesis that this series of compounds operates via a distinct mechanism of

action to that of ezutromid. Interestingly, ATP5F1 (subunit b of mitochondrial ATP synthase) was identified as a target by the active probe **64** against both inactive and competitor controls. Oxidative metabolism and ATP synthesis are known to be severely compromised in DMD pathology [22–25], while induction of slower oxidative muscle phenotypes through small molecule regulation of oxidative respiration and metabolism have been shown in preclinical trials to upregulate utrophin and mitigate dystrophic pathology [26–28]. A protein network database search [29,30] suggested that ATP5F1 expression and activity are not mediated by AhR; the effects of targeting ATP5F1 on mitochondrial function and utrophin regulation in DMD cells will form the basis of future studies.

## Conclusions

A cell-based phenotypic reporter gene assay exploiting the full utrophin promoter was developed by knock-in of firefly luciferase into one utrophin exon 7 allele in a dystrophin-null mouse (*LUmdx*). Screening of compounds in an immortalised myoblast *LUmdx* cell line led to discovery of a novel class of utrophin modulators based on the original hit molecule 4,6-diphenylpyrimidine-2-carbohydrazide (OX01914, **1**). OX01914 was further found to upregulate utrophin mRNA in *LUmdx* myoblasts and protein in human DMD myoblasts. The inactivity of OX01914 in the H2K-*mdx* utrA-luc phenotypic screen in which ezutromid was discovered, along with its null effect on AhR-mediated gene expression indicate that this class of compounds operate via a distinct mechanism of action.

Synthesis of 43 analogues with systematic variations of the head group, core and peripheral substituents led to a fuller understanding of the structure-activity relationship of OX01914. While the majority of alterations diminished activity, many *para*-substituents on the phenyl rings led to more potent analogues. The SAR of the series inspired the design and synthesis of active and inactive cell-permeable photoaffinity probes to deconvolute the protein targets of OX01914. Identification of probe-binding proteins in live human DMD myoblasts by LC-MS/MS confirmed that AhR is not a target of OX01914, while highlighting ATP5F1 as a target to be further explored. Taken together, these findings reveal 4,6-diphenylpyrimidine-2-carbohydrazides as novel utrophin modulators worthy of further investigation for the treatment of Duchenne muscular dystrophy.

## Acknowledgements

The authors wish to thank Summit Therapeutics plc (M.C., D.C., N.S.), the Medical Research Council (EP/L016044/1, I.V.L.W.; 1501AV003/CA2, B.E., S.E.S, K.E.D.), the Engineering and Physical Sciences Research Council (EP/L016044/1, I.V.L.W.), Muscular Dystrophy Association (MDA212606, J.R.D., N.A.B.), Duchenne UK (N.A.B.) and Muscular Dystrophy UK (RA4/3013/4, A.V.) for financial support. We thank G. E. Morris (Oswestry, UK) for the gift of the utrophin A MANCHO3 antibody. The authors gratefully acknowledge Aurelia Bioscience (UK) for performing the firefly luciferase inhibition and dual luciferase (Firefly/Renilla) CMV reporter assays; Cyprotex Discovery Ltd (U.K.) for the physicochemical and ADME evaluation; Key Organics (particularly Steve Brough and Becky Gill) for analogue synthesis and helpful input to the route design.

## Conflict of interest

R.J.F., S.G.D., A.J.R. and K.E.D are minor shareholders of Summit Therapeutics plc.

## Abbreviations

A→B – apical to basolateral transport

ADME – absorption, distribution, metabolism, and excretion

AhR – aryl hydrocarbon receptor  
CuAAC – copper-catalysed azide-alkyne cycloaddition  
DMD – Duchenne muscular dystrophy  
ER – efflux ratio  
hHep – human hepatocytes  
IA – inactive, where  $EC_{50} > 100 \mu\text{M}$   
LC-MS/MS – liquid chromatography-tandem mass spectrometry  
mHep – mouse hepatocytes  
PEG – polyethylene glycol  
SAR – structure-activity relationship  
SDS-PAGE – sodium dodecyl sulfate polyacrylamide gel electrophoresis  
SEM – standard error of the mean  
TAMRA – tetramethylrhodamine  
TPD – trifluoromethylphenyl diazirine

## References

- [1] S. Guiraud, K.E. Davies, Pharmacological advances for treatment in Duchenne muscular dystrophy, *Curr. Opin. Pharmacol.* 34 (2017) 36–48. <https://doi.org/10.1016/J.COPH.2017.04.002>.
- [2] S. Guiraud, D. Roblin, K.E. Davies, The potential of utrophin modulators for the treatment of Duchenne muscular dystrophy, *Expert Opin. Orphan Drugs.* 6 (2018) 179–192. <https://doi.org/10.1080/21678707.2018.1438261>.
- [3] D.R. Chancellor, K.E. Davies, O. De Moor, C.R. Dorgan, P.D. Johnson, A.G. Lambert, D. Lawrence, C. Lecci, C. Maillol, P.J. Middleton, G. Nugent, S.D. Poignant, A.C. Potter, P.D. Price, R.J. Pye, R. Storer, J.M. Tinsley, R. van Well, R. Vickers, J. Vile, F.J. Wilkes, F.X. Wilson, S.P. Wren, G.M. Wynne, Discovery of 2-Arylbenzoxazoles as Upregulators of Utrophin Production for the Treatment of Duchenne Muscular Dystrophy, *J. Med. Chem.* 54 (2011) 3241–3250. <https://doi.org/10.1021/jm200135z>.
- [4] J.M. Tinsley, R.J. Fairclough, R. Storer, F.J. Wilkes, A.C. Potter, S.E. Squire, D.S. Powell, A. Cozzoli, R.F. Capogrosso, A. Lambert, F.X. Wilson, S.P. Wren, A. De Luca, K.E. Davies, Daily Treatment with SMT C1100, a Novel Small Molecule Utrophin Upregulator, Dramatically Reduces the Dystrophic Symptoms in the mdx Mouse, *PLoS One.* 6 (2011) e19189. <https://doi.org/10.1371/journal.pone.0019189>.
- [5] M. Chatzopoulou, T.D.W. Claridge, K.E. Davies, S.G. Davies, D.J. Elsey, E. Emer, A.M. Fletcher, S. Harriman, N. Robinson, J.A. Rowley, A.J. Russell, J.M. Tinsley, R. Weaver, I.V.L. Wilkinson, N.J. Willis, F.X. Wilson, G.M. Wynne, Isolation, Structural Identification, Synthesis, and Pharmacological Profiling of 1,2-trans-Dihydro-1,2-diol Metabolites of the Utrophin Modulator Ezutromid, *J. Med. Chem.* 63 (2019) 2547–2556. <https://doi.org/10.1021/acs.jmedchem.9b01547>.
- [6] V. Ricotti, S. Spinty, H. Roper, I. Hughes, B. Tejura, N. Robinson, G. Layton, K. Davies, F. Muntoni, J. Tinsley, Safety, Tolerability, and Pharmacokinetics of SMT C1100, a 2-Arylbenzoxazole Utrophin Modulator, following Single- and Multiple-Dose Administration to Pediatric Patients with Duchenne Muscular Dystrophy, *PLoS One.* 11 (2016) e0152840. <https://doi.org/10.1371/journal.pone.0152840>.
- [7] A. Braeuning, Firefly luciferase inhibition: a widely neglected problem, *Arch. Toxicol.* 89 (2015) 141–142. <https://doi.org/10.1007/s00204-014-1423-3>.
- [8] I.V.L. Wilkinson, J.K. Reynolds, S.R.G. Galan, A. Vuorinen, A.J. Sills, E. Pires, G.M. Wynne, F.X. Wilson, A.J. Russell, Characterisation of utrophin modulator SMT C1100

- as a non-competitive inhibitor of firefly luciferase, *Bioorg. Chem.* 94 (2020) 103395. <https://doi.org/10.1016/j.bioorg.2019.103395>.
- [9] I.V.L. Wilkinson, K.J. Perkins, H. Dugdale, L. Moir, A. Vuorinen, M. Chatzopoulou, S.E. Squire, S. Monecke, A. Lomow, M. Geese, P.D. Charles, P. Burch, J.M. Tinsley, G.M. Wynne, S.G. Davies, F.X. Wilson, F. Rastinejad, S. Mohammed, K.E. Davies, A.J. Russell, Chemical Proteomics and Phenotypic Profiling Identifies the Aryl Hydrocarbon Receptor as a Molecular Target of the Utrophin Modulator Ezutromid, *Angew. Chemie - Int. Ed.* 59 (2020) 2420–2428. <https://doi.org/10.1002/anie.201912392>.
- [10] F. Lovering, J. Bikker, C. Humblet, Escape from flatland: Increasing saturation as an approach to improving clinical success, *J. Med. Chem.* 52 (2009) 6752–6756. <https://doi.org/10.1021/jm901241e>.
- [11] I.V.L. Wilkinson, K.J. Perkins, H. Dugdale, L. Moir, A. Vuorinen, M. Chatzopoulou, S.E. Squire, S. Monecke, A. Lomow, M. Geese, P.D. Charles, P. Burch, J.M. Tinsley, G.M. Wynne, S.G. Davies, F.X. Wilson, F. Rastinejad, S. Mohammed, K.E. Davies, A.J. Russell, Chemical Proteomics and Phenotypic Profiling Identifies the Aryl Hydrocarbon Receptor as a Molecular Target of the Utrophin Modulator Ezutromid, *Angew. Chemie Int. Ed.* (2019). <https://doi.org/10.1002/anie.201912392>.
- [12] K.M. Comess, S.M. McLoughlin, J.A. Oyer, P.L. Richardson, H. Stöckmann, A. Vasudevan, S.E. Warder, Emerging Approaches for the Identification of Protein Targets of Small Molecules - A Practitioners' Perspective, *J. Med. Chem.* 61 (2018) 8504–8535. <https://doi.org/10.1021/acs.jmedchem.7b01921>.
- [13] I.V.L. Wilkinson, G.C. Terstappen, A.J. Russell, Combining experimental strategies for successful target deconvolution, *Drug Discov. Today.* (2020). <https://doi.org/10.1016/j.drudis.2020.09.016>.
- [14] M.H. Wright, S.A. Sieber, Chemical proteomics approaches for identifying the cellular targets of natural products., *Nat. Prod. Rep.* 33 (2016) 681–708. <https://doi.org/10.1039/c6np00001k>.
- [15] E. Smith, I. Collins, Photoaffinity labeling in target- and binding-site identification, *Future Med. Chem.* 7 (2015) 159–183. <https://doi.org/10.4155/fmc.14.152>.
- [16] J.R. Hill, A.A.B. Robertson, Fishing for Drug Targets: A Focus on Diazirine Photoaffinity Probe Synthesis, *J. Med. Chem.* 61 (2018) 6945–6963. <https://doi.org/10.1021/acs.jmedchem.7b01561>.
- [17] R.D. Row, J.A. Prescher, Constructing New Bioorthogonal Reagents and Reactions, *Acc. Chem. Res.* 51 (2018) 1073–1081. <https://doi.org/10.1021/acs.accounts.7b00606>.
- [18] C.J. Pickens, S.N. Johnson, M.M. Pressnall, M.A. Leon, C.J. Berkland, Practical Considerations, Challenges, and Limitations of Bioconjugation via Azide-Alkyne Cycloaddition, *Bioconjug. Chem.* 29 (2018) 686–701. <https://doi.org/10.1021/acs.bioconjchem.7b00633>.
- [19] C.M. Timmers, H.J.J. Loozen, H.T. Stock, Ring-annulated dihydropyrrolo[2,1- $\alpha$ ]isoquinolines, US 2011 0028450 A1, 2011.
- [20] J. Bucher, T. Wurm, K.S. Nalivela, M. Rudolph, F. Rominger, A.S.K. Hashmi, Cyclization of Gold Acetylides: Synthesis of Vinyl Sulfonates via Gold Vinylidene Complexes, *Angew. Chemie Int. Ed.* 53 (2014) 3854–3858. <https://doi.org/10.1002/anie.201310280>.

- [21] R. Mori, A. Kato, K. Komenoi, H. Kurasaki, T. Iijima, M. Kawagoshi, Y.B. Kiran, S. Takeda, N. Sakai, T. Konakahara, Synthesis and in vitro antitumor activity of novel 2-alkyl-5-methoxycarbonyl-11-methyl-6H-pyrido[4,3-b]carbazol-2-ium and 2-alkylellipticin-2-ium chloride derivatives, *Eur. J. Med. Chem.* 82 (2014) 16–35. <https://doi.org/10.1016/j.ejmech.2014.05.032>.
- [22] A. V. Kuznetsov, K. Winkler, F.R. Wiedemann, P. Von Bossanyi, K. Dietzmann, W.S. Kunz, Impaired mitochondrial oxidative phosphorylation in skeletal muscle of the dystrophin-deficient mdx mouse, *Mol. Cell. Biochem.* 183 (1998) 87–96. <https://doi.org/10.1023/A:1006868130002>.
- [23] J.M. Percival, M.P. Siegel, G. Knowels, D.J. Marcinek, Defects in mitochondrial localization and ATP synthesis in the mdx mouse model of duchenne muscular dystrophy are not alleviated by PDE5 inhibition, *Hum. Mol. Genet.* 22 (2013) 153–167. <https://doi.org/10.1093/hmg/dds415>.
- [24] E. Rybalka, C.A. Timpani, M.B. Cooke, A.D. Williams, A. Hayes, Defects in mitochondrial ATP synthesis in dystrophin-deficient Mdx skeletal muscles may be caused by complex I insufficiency, *PLoS One.* 9 (2014) e115763. <https://doi.org/10.1371/journal.pone.0115763>.
- [25] D. Capitano, M. Moriggi, E. Torretta, P. Barbacini, S. De Palma, A. Viganò, H. Lochmüller, F. Muntoni, A. Ferlini, M. Mora, C. Gelfi, Comparative proteomic analyses of Duchenne muscular dystrophy and Becker muscular dystrophy muscles: changes contributing to preserve muscle function in Becker muscular dystrophy patients, *J. Cachexia. Sarcopenia Muscle.* 11 (2020) 547–563. <https://doi.org/10.1002/jcsm.12527>.
- [26] V. Ljubicic, P. Miura, M. Burt, L. Boudreault, S. Khogali, J.A. Lunde, J.-M. Renaud, B.J. Jasmin, Chronic AMPK activation evokes the slow, oxidative myogenic program and triggers beneficial adaptations in mdx mouse skeletal muscle, *Hum. Mol. Genet.* 20 (2011) 3478–3493. <https://doi.org/10.1093/hmg/ddr265>.
- [27] C. Péladeau, A. Ahmed, A. Amirouche, T.E. Crawford Parks, L.M. Bronicki, V. Ljubicic, J.-M. Renaud, B.J. Jasmin, Combinatorial therapeutic activation with heparin and AICAR stimulates additive effects on utrophin A expression in dystrophic muscles., *Hum. Mol. Genet.* 25 (2016) 24–43. <https://doi.org/10.1093/hmg/ddv444>.
- [28] P. Miura, J. V. Chakkalakal, L. Boudreault, G. Belanger, R.L. Hebert, J.-M. Renaud, B.J. Jasmin, Pharmacological activation of PPAR $\beta/\delta$  stimulates utrophin A expression in skeletal muscle fibers and restores sarcolemmal integrity in mature mdx mice, *Hum. Mol. Genet.* 18 (2009) 4640–4649. <https://doi.org/10.1093/hmg/ddp431>.
- [29] STRING: functional protein association networks, (n.d.). <https://string-db.org/> (accessed April 15, 2020).
- [30] A.D. Rouillard, G.W. Gunderson, N.F. Fernandez, Z. Wang, C.D. Monteiro, M.G. McDermott, A. Ma'ayan, The harmonizome: a collection of processed datasets gathered to serve and mine knowledge about genes and proteins, *Database (Oxford).* 2016 (2016). <https://doi.org/10.1093/database/baw100>.